ACS NANO
Cite This: ACS Nano 2019, 13, 5541−5548
www.acsnano.org

ARTICLE

Transfer-Medium-Free Nanofiber-Reinforced Graphene Film and Applications in Wearable Transparent Pressure Sensors

Huaying Ren,[†,‡] Liming Zheng,[†] Guorui Wang,[§] Xin Gao,[†] Zhenjun Tan,[†] Jingyuan Shan,[†,‡] Lingzhi Cui,[†] Ke Li,[∥] Muqiang Jian,[∥,⊥] Liangchao Zhu,[¶] Yingying Zhang,[⊥] Hailin Peng,*[,†,∥] Di Wei,*[,†,∥] and Zhongfan Liu*[,†,∥]

[†]Center for Nanochemistry, College of Chemistry and Molecular Engineering, and [‡]Academy for Advanced Interdisciplinary Studies, Peking University, Beijing 100871, China

[§]CAS Key Laboratory of Nanosystem and Hierarchical Fabrication, CAS Center for Excellence in Nanoscience, National Center for Nanoscience and Technology, Beijing 100190, China

[∥]Beijing Graphene Institute, Beijing 100094, China

[⊥]Department of Chemistry and Center for Nano and Micro Mechanics, Tsinghua University, Beijing 100084, China

[¶]State Key Laboratory of CAD&CG, Zhejiang University, Hangzhou 310058, China

Supporting Information

ABSTRACT: **Graphene exhibits properties of atomic thickness, high transparency, and high carrier mobility, which is highly desirable for a flexible transparent conductive material. However, the electronic properties of large-area chemical vapor deposition grown graphene film suffer from insulated polymer contaminations introduced by the transfer process and the easily cracked nature. Here, we report a preparation method of a transfer-medium-free large-area nanofiber-reinforced graphene (a-PAN/G) film simply by annealing the electrostatically spun polyacrylonitrile (PAN) nanofibers on the graphene film. The film could be free-standing on water and suspended in air with high transparency and enhanced electrical and mechanical properties compared to that of a monolayer graphene film. The flexible transparent a-PAN/G films were demonstrated as active materials for sensitive pressure sensors. The obtained pressure sensors demonstrate high sensitivity (44.5 kPa^{-1} within 1.2 kPa), low operating voltage (0.01−0.5 V), and excellent stability for 5500 loading−unloading cycles, revealing promising potential applications in wearable electronics.**

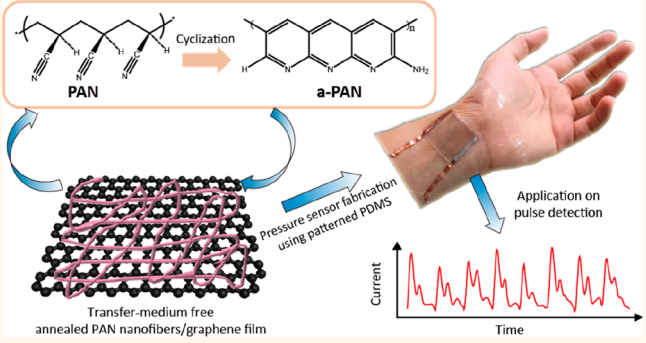

KEYWORDS: *graphene, polyacrylonitrile nanofibers, graphene transfer, electrospinning, chemical vapor deposition, conductive transparent film, flexible pressure sensor*

Flexible transparent conductive film, as a vital part of recently emerging wearable electronics, has important applications in soft and flexible displays,[1,2] transparent transistors,[3−5] energy sources,[6−8] radio frequency identification devices (RFIDs),[9−11] and pressure/strain sensors.[12−16] Graphene, a two-dimensional material composed of sp^2-hybridized carbon atoms, possesses many demanded properties such as high transparency (97.7%), high carrier mobility (2×10^5 cm^2·V^{-1}·s^{-1} at room temperature in theory), and flexibility due to its atomic thickness. Chemical vapor deposition (CVD) is a relatively developed technology to grow large-area and high-quality graphene films.[2,17,18] The optical and electrical properties of CVD graphene are comparable with the ideal ones,[17−20] which makes it a very competitive material for devices involving flexible transparent conductive film.

Despite the huge advantages that CVD graphene has shown, the conductivity decreases owing to limited fracture toughness properties[21−23] and polymer residues,[21,24,25] inhibiting the performances of its applications in wearable flexible transparent devices. To fabricate devices using large-area CVD graphene films, a transfer process is usually needed because commonly used growth substrate copper foils are neither soft nor

Received: January 15, 2019
Accepted: April 29, 2019
Published: April 29, 2019

DOI: 10.1021/acsnano.9b00395
ACS Nano 2019, 13, 5541−5548

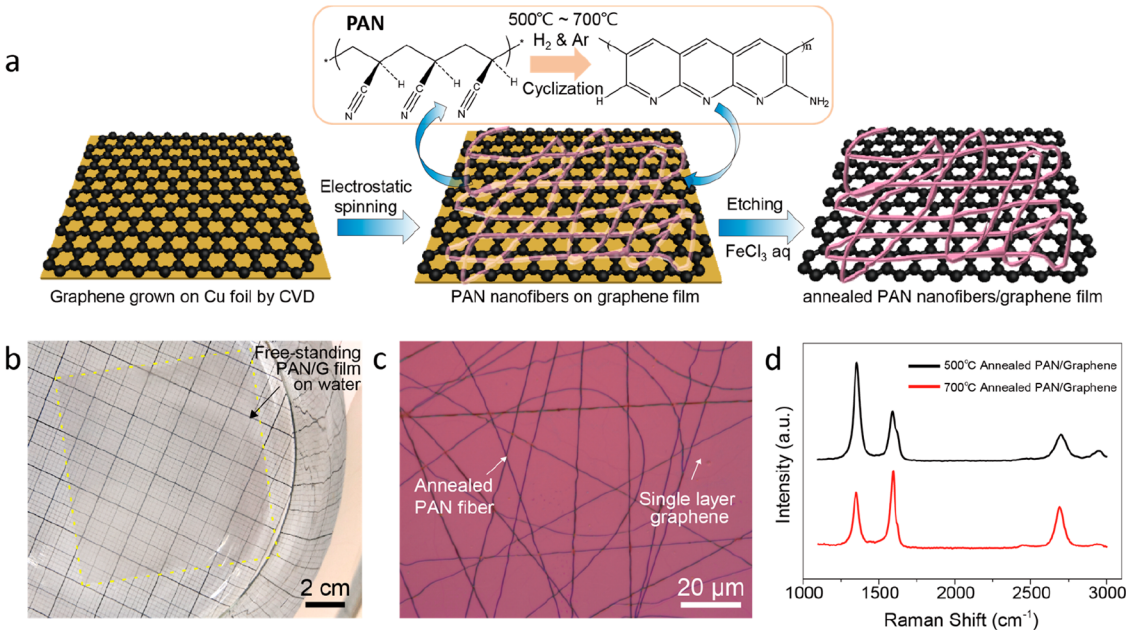

Figure 1. Schematics and characterizations of a-PAN/G film. (a) Schematic of the fabrication procedure for a-PAN/G film. PAN nanofibers went through cyclization and a partial carbonization reaction during the annealing process. After being etched and washed, the a-PAN/G film was spread on ultrapure water without other supporting material. (b) Photograph of a-PAN/G film on water after being washed. (c) Optical microscope image of a-PAN/G film transferred onto a SiO_2/Si slice (300 nm SiO_2 layer). (d) Raman spectra of a-PAN/G films with different annealing temperatures.

transparent and unfit to be used as target substrates. On one hand, large-area graphene without any assisted supporting material would be easily cracked or wadded during the transfer process.[21,23,26] On the other hand, graphene film obtained by a polymer-assisted transfer process usually needs to remove the introduced polymer layer such as poly(methyl methacrylate) (PMMA), polydimethylsiloxane (PDMS), rosin, and *etc.*[2,27,28] However, there were some amounts of dielectric polymer residues remaining on the graphene surface. Therefore, the mechanical and electronic properties of CVD graphene are degraded. Efforts have been focused on these problems, and a number of methods were reported recently. For example, graphene nanoscrolls between stacked graphene layers could bridge the fragmented graphene domains to maintain a conductive network, which enabled excellent conductivity at high deformations.[3] Nonetheless, the film still needs to be transferred several times with the assistance of a polymer. Quite a few works have reported using carbon nanotubes (CNTs) as supporting material to reinforce the graphene films.[13,14,29] These CNTs/graphene composite films could be quite robust, whereas a redundant and complicated CVD-grown process was required to gain CNTs. In addition, few of these film-making methods could achieve the goal of polymer-free transfer. A convenient and efficient way toward higher mechanical strength, better conductivity, and transparent graphene-based films is urgently needed.

To solve these problems mentioned above, we designed and fabricated an annealed polyacrylonitrile nanofiber/graphene (a-PAN/G) composite film. PAN nanofibers were simply spun on the CVD graphene film by electrospinning and annealing afterward. Taking advantage of the cyclization reaction of PAN, we could transfer this a-PAN/G film to various substrates without any assistance of a medium, which helps a lot to preserve and further enhance graphene's excellent properties, such as high conductivity and flexibility. Meanwhile, the gridding structure of annealed PAN nanofibers guarantees the transparency of the whole film (≥94%). Transparent and flexible pressure/strain sensors play key roles in wearable electronics for their important function of original data acquirement. As an active material, the conductivity and transparency of graphene films make them very promising for use as sensors. Due to the improved structural integrity of the a-PAN/G film, a flexible transparent pressure sensor was explored using the a-PAN/G film as an active material. The sensor exhibited high sensitivity of 44.5 kPa^{-1} within 1.2 kPa and excellent stability for more than 5000 loading−unloading cycles under 0.6 kPa. The sensor is operated under low operating voltage (0.01−0.5 V) with extremely low energy consumption. In addition, the sensing area of the device is highly transparent to observe things underneath. We demonstrated applications of the transparent flexible sensor for pulse measurement, acoustic vibrations, and slight pressures, illustrating the promising potential applications in wearable electronics of this a-PAN/G film.

RESULTS AND DISCUSSION

To ensure the large area and high quality of transparent flexible conductive films, a graphene film consisting of large-sized single-crystal domains was synthesized on copper foil by a CVD multistage precursor supply method developed previously.[30,31] The PAN nanofibers were electrostatically spun on the surface of graphene using 8 wt % PAN in dimethylformamide (DMF), and subsequently, the PAN/graphene/copper foil were annealed under a mixed atmosphere of argon (300−500 sccm) and hydrogen (50−100 sccm). As shown in Figure 1a, during the annealing process, the PAN nanofibers were going through cyclization and aromatization reactions at a temperature of 500 °C and graphitization at a higher temperature.[32,33] Conjugated structures were acquired in these annealed PAN nanofibers and helped the fibers attach

DOI: 10.1021/acsnano.9b00395
ACS Nano 2019, 13, 5541−5548

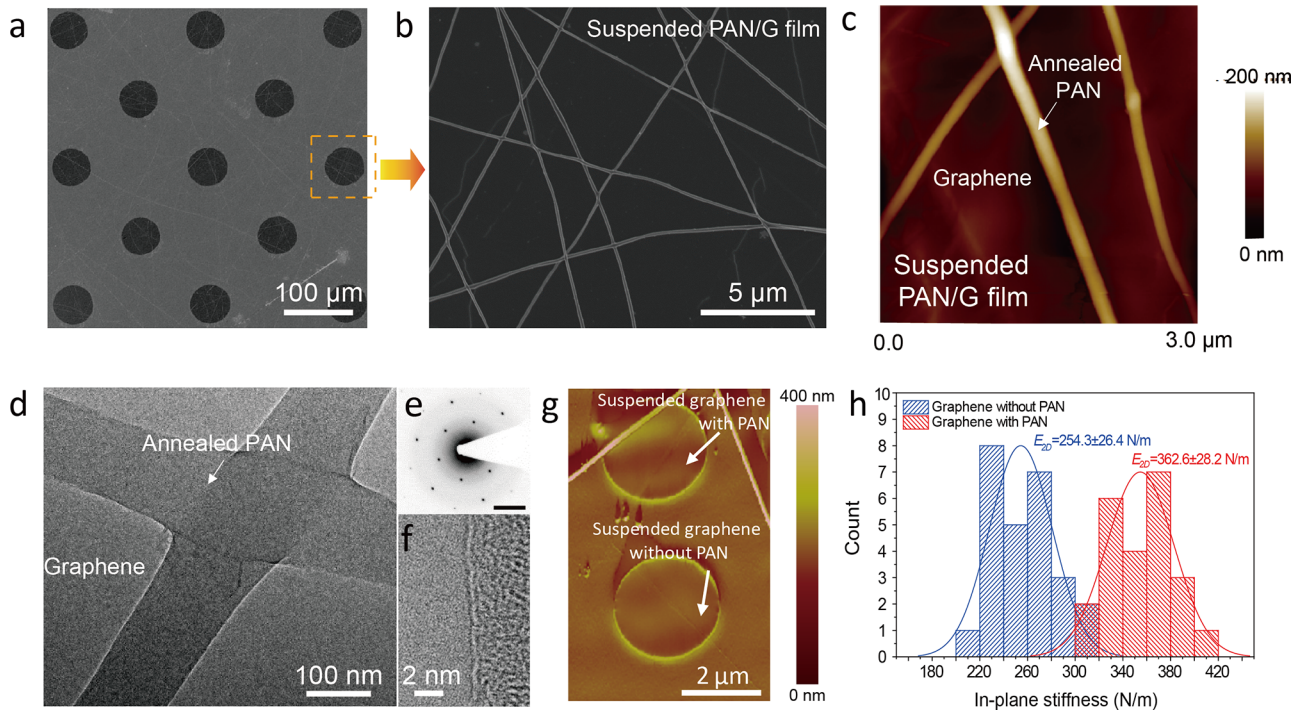

Figure 2. Characterizations of suspended a-PAN/G film. (a) SEM image of highly intact a-PAN/G film on the copper substrate with periodic holes. Diameter of holes: 55 μm. (b) SEM image of suspended a-PAN/G film taken from one of the holes in (d). (c) Typical AFM height-mode image of suspended a-PAN/G film. (d) Typical TEM micrographs of a suspended annealed PAN fiber junction on graphene film. (e) SAED pattern of the graphene area. Scale bar is 5 nm^{-1}. (f) High-resolution transmission electron microscopy micrograph showing the graphene film is a monolayer. (g) AFM image of holes of the film; diameter of each hole is 2.5 μm. (h) Histogram of elastic stiffness of graphene film with and without PAN nanofibers.

onto the graphene surface tightly by $\pi-\pi$ interaction. A copper substrate could be etched directly by simply putting the as-annealed PAN/G film on the $FeCl_3$ solution. Note that the nanofiber-reinforced graphene film was free from any other polymer assistance, such as PMMA, and was able to withstand the washing process. This transparent flexible film was well spread on the water and could be transferred onto various substrates for corresponding applications.

Figure 1b shows that a-PAN/G was floating on ultrapure water after being etched and washed. Usually, graphene films without polymer coating rarely spread on the water due to the surface tension of water, which will cause the graphene domains to roll up into scrolls. However, the floating size of the a-PAN/G film could be up to about 9.5 cm × 9.5 cm, representing a major advance compared with conventional PMMA-based graphene film. The a-PAN/G film after annealing was a large-area, continuous graphene film with junction-fused nanofibers on it. The transferred film on the SiO_2/Si substrate could be observed directly by an optical microscope (Figure 1c). Clearly, there was no crack on the high-quality graphene film. As shown in Figure 1d, after the transfer, Raman spectra of film samples with different annealing temperatures were selected, showing the mixed signal of annealed PAN nanofibers and monolayer graphene film. Unless otherwise specified, the a-PAN/G films used afterward were all annealed under 700 °C.

It is shown in Figure 2a,b that the a-PAN/G film was highly intact on the copper substrate with periodic holes and suspension in air. The diameter of the holes is 55 μm. Atomic force microscopy (AFM) characterizations of the a-PAN/G suspended film showed that the diameter of the fibers was in the range of 90−250 nm (Figure 2c and Figure S1), and the fibers were tightly attached to the graphene films underneath, helping preserve the film shape and integrity during the processes of etching and transfer. The shape and diameters of annealed PAN nanofibers could also be gained from the transmission electron microscopy (TEM) images of the suspended a-PAN/G film (Figure 2d and Figure S2). Fusion of annealed PAN nanofiber junctions could be observed in these images. The fusion of junctions made the fibers a whole network to form a composite film with mechanical integrity and further facilitated the electrical conduction. Selected area electron diffraction (SAED) revealed a single set of hexagonal symmetry (Figure 2e), demonstrating that the graphene of the selected area was single-crystalline. The graphene monolayer nature was shown by an inner peak intensity of the diffraction pattern that was stronger than that of outer peaks (Figure S3), as well as the high-resolution TEM image of the accurate layer at the film edge (Figure 2f). Partial carbonization of nanofibers after being annealed at 700 °C was indicated by ring patterns of amorphous carbon SAED (Figure S3).

The network composed by annealed PAN nanofibers had multiple functions to the whole film, such as mechanical reinforcement and electrical conductivity improvement. Using nanoindentation on a suspended a-PAN/G film (Figure S4 and Figure 2g), elastic stiffness of a-PAN/G film and G film in a 2.5 μm hole could be calculated from the data of loading curves and curve fittings (Figure S5). For a-PAN/G film, the calculated elastic stiffness was 362.6 ± 28.2 N/m and that of G film was 254.3 ± 26.4 N/m (Figure 2h and Figure S5). Referring to previous calculation methods,[34,35] the calculated Young's moduli of the film with and without annealed PAN

DOI: 10.1021/acsnano.9b00395
ACS Nano 2019, 13, 5541−5548

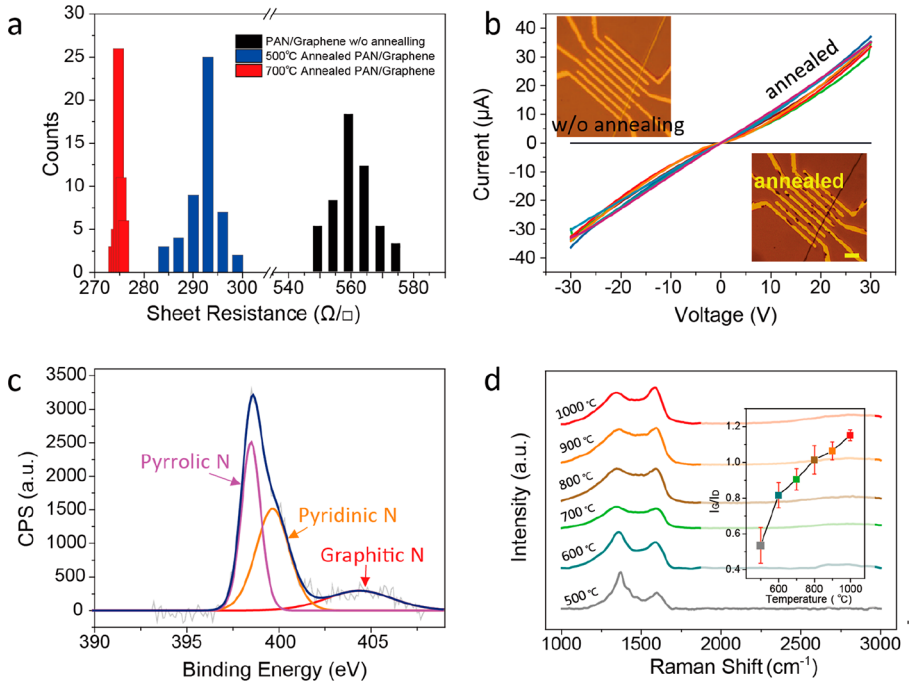

Figure 3. Conductivity increase with annealed PAN fibers. (a) Sheet resistance distributions of a-PAN/G film with 700 °C (red), 500 °C (blue), and without (black) annealing. Average sheet resistances of different a-PAN/G films were 275 Ω/□ (annealed at 700 °C), 294 Ω/□ (annealed at 500 °C), and 563 Ω/□ (without annealing). (b) *I*−*V* curve of PAN nanofibers with and without annealing. Insets are images of PAN fibers with or without annealing taken from an optical microscope. Scale bar is 10 μm. (c) N 1s X-ray photoelectron spectra of the a-PAN/G film annealed at 700 °C. The N 1s peak is split into three Lorentzian peaks at 404.5 eV (red), 399.7 eV (orange), and 398.2 eV (purple), which represent graphic, pyridinic, and pyrrolic N, respectively. (d) Raman spectra of PAN nanofibers annealed at different temperatures. Inset is the G peak and D peak intensity ratios *versus* annealing temperature, corresponding to the Raman spectra on the left.

fibers were 1.04 ± 0.08 TPa and 747.9 ± 77.6 GPa, respectively (Table S1). Details of the indentation process and calculation of the elastic modulus are provided in the Supporting Information. It indicated that PAN fibers helped to enhance the elastic stiffness in the local area, acting like steel bars in concrete. It can be seen through the comparison of the calculated Young's modulus[34−37] (Table S1) that the a-PAN/G film in this work had excellent mechanical strength, which is comparable to and even stronger than that of the defect-free exfoliated graphene flakes.

For the conductivity, Figure 3a shows that the sheet resistance of the a-PAN/G film before annealing was around 563 Ω/□, which was similar to that of an intrinsic graphene monolayer.[30,31] It is shown that the a-PAN/G film annealed under 500 and 700 °C had better conductivities, with sheet resistances of 294 and 275Ω/□, respectively. The distribution of sheet resistance was narrower along with the increase of annealing temperature. An annealed PAN fiber network might provide additional pathways for electron transportation, avoiding the imperfect grain boundaries (Figure S6), and may also play the role of dopant to graphene.

To confirm the increase in conductivity of annealed PAN fibers, *in situ* electrical measurements were conducted. PAN fibers were electrostatically spun onto six preset SiO_2/Si electrode wafer slices. After measurement of currents under sweep voltages from −30 to +30 V in 60 channels, the slices were annealed at 500 °C (a temperature higher than 500 °C would damage the electrodes), and the currents were measured in the same way (Figure 3b). Statistical distribution of the channel resistance is shown in Figure S7; the average resistance decreased from ∼2.8 × 10^8 to ∼910 Ω, which was in line with the reaction principle that dielectric long chain saturated polymers cyclize and form a delocalized π bond by annealing. Figure 3c and Figure S8 show N 1s X-ray photoelectron spectra of a-PAN/G film and PAN fibers annealed under different temperatures. The nitrogen content of nanofibers had been decreasing consistently with the increasing annealing temperature, and at the higher temperature of 700 °C, the graphitic nitrogen began to arise. It is revealed by Raman spectra (Figure 3d) that the increasing annealing temperature also leads to a graphitization process in nanofibers as the peak intensity ratios, I_G/I_D, and the shape of the peaks appear more like amorphous carbon at an annealing temperature greater than 700 °C.

The mechanical-integrity-reinforced and electrical-conduction-enhanced a-PAN/G flexible conductive film could serve a number of purposes. In our case, we used the a-PAN/G film as an active material in transparent flexible pressure sensors. In our design, the devices were fabricated using two layers of 700 °C annealed a-PAN/G film combined with microstructurally patterned PDMS (p-PDMS), and the schematic depictions of the device are shown in Figure 4a. The a-PAN/G/p-PDMS films were placed face to face, and the wires were bonded by silver paste on opposite edges of each film. In this pressure sensor design, two layers of a-PAN/G/p-PDMS films contacted partially at the initial state, further under a certain given pressure, and totally under pressure of the detection limit (Figure S9). This series of deformation causes increased conductive paths and decreased electrical resistance and thus implement pressure detection.

Apart from the requirements for graphene film to be used as active materials mentioned above, the structure design of the

DOI: 10.1021/acsnano.9b00395
ACS Nano 2019, 13, 5541−5548

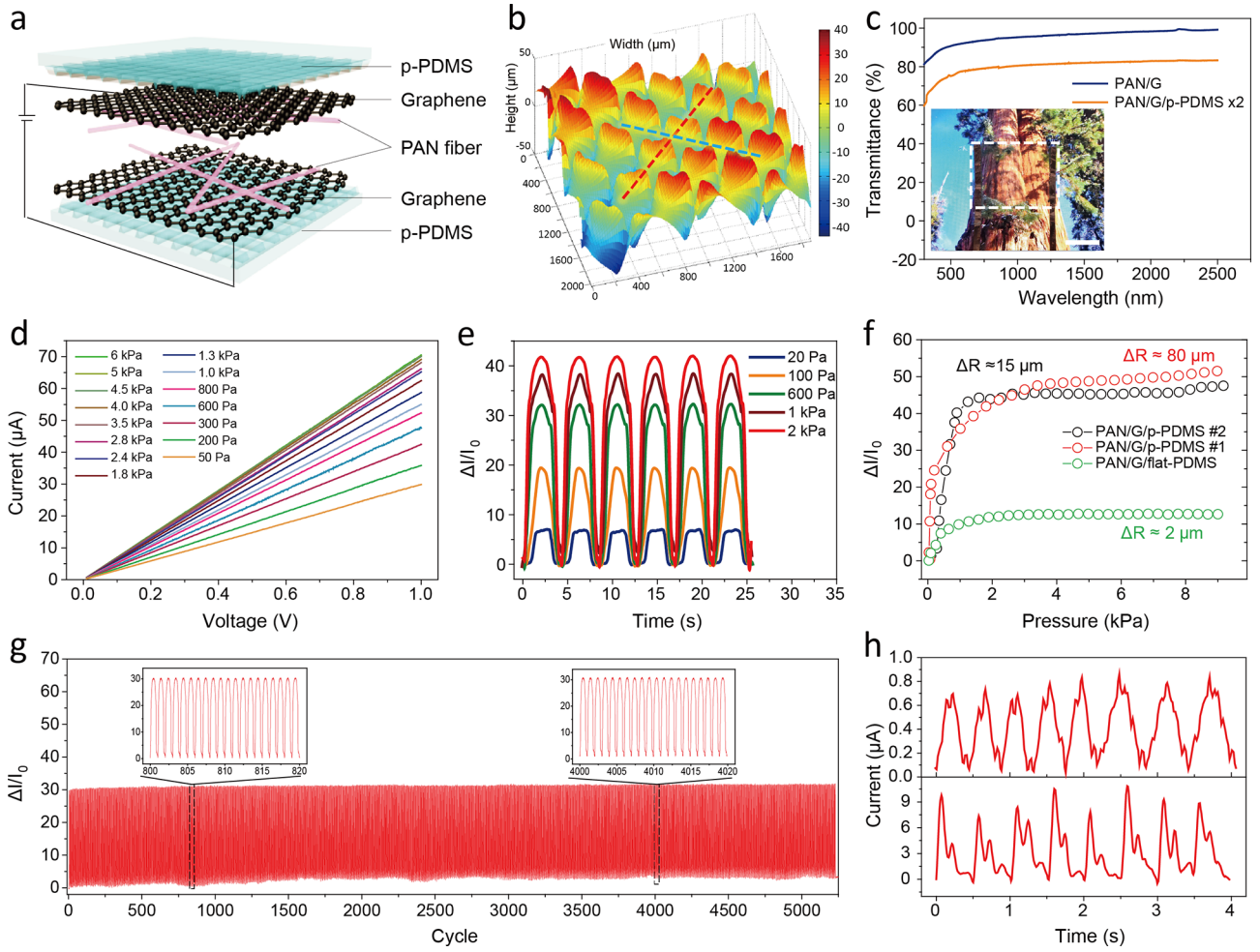

Figure 4. Demonstration of PAN/G-film-based transparent flexible pressure sensors. (a) Schematic of a double layer a-PAN/G/PDMS constructed pressure sensor with a description of each layer. (b) 3D profile mapping of PDMS substrate with pattern #1 measured by a 3D optical surface profiler. Scale of color bar is μm. (c) Transmittances of a-PAN/G film and double layered a-PAN/G/PDMS. Inset is the photograph of an as-fabricated a-PAN/G-based pressure sensor. Scale bar: 1 cm. (d) $I-V$ curves under static pressures from 50 to 6000 Pa. (e) Changes in current under periodic loading pressure ranging from 20 to 2000 Pa, 0.5 V. (f) Pressure response curves of pressure sensors with different surface roughness in the range of 0−9 kPa, 0.5 V. (g) Total of 5500 loading−unloading cycle durability tests under 0.6 kPa, 0.5 V. (h) Measurement data of the pulse of a human radial artery on the wrist without (top plot) and with (bottom plot) transparent polyurethane dressing under constant operating voltage of 0.5 V.

elastic substrate is also of vital importance in many flexible devices. For piezoresistive sensors, sensitivity depends on the resistance variation (ΔR) under different applied pressures and initial current (I_0). Microstructures on substrates help reduce the contact area in the initial state while providing greater contact area changes in the operating state, which will in turn decrease I_0 and increase ΔR of the device. This was well-illustrated by some early work using flexible substrates with micropyramid, microdome, and interlocking microstructure arrays.[38−40] The reverse mold for substrate patterning was usually obtained *via* a complex set of lithography processes, which is costly and time-consuming. To simplify the fabrication process of substrates, natural leaves, silk, *etc.* served as molds to create the defined structures.[13,16] For these methods, high cost, small-area molds, and irregular variation range became the major constraints, which impeded the large-scale and extensive use of the substrate.

For improvement, a scalable and reusable p-PDMS template fabrication process was proposed (shown in Figure S10). The inverted structured template could be obtained simply by putting copper foil into the prepatterned commercial vacuum sealer bag and extruding the foil to copy the structure by vacuum. We chose two kinds of periodical patterns with a roughness of ±40 μm (Figure 4b and Figure S11) and ±7.5 μm (Figure S12), named pattern #1 and pattern #2. The surface of p-PDMS with pattern #1 showed a criss-cross alternate peak (~40 μm high) and valleys (~40 μm deep) (Figure S11), while the surface of p-PDMS with pattern #2 presents a smaller zigzag pattern. The height difference of pattern #2 after baseline calibration was about 14 μm. As shown in Figure 4c, the transmittance of the a-PAN/G film and the two layered a-PAN/G/p-PDMS pressure sensor at 600 nm was 94 and 77%, respectively. The gridding structure of annealed PAN nanofibers had little influence on the transparency of graphene films. Using these transparent films, the as-fabricated pressure sensor also showed high transparency, so that the picture behind the device could be recognized clearly (inset of Figure 4c).

To test the performance of the a-PAN/G-based transparent flexible pressure sensors under static and dynamic pressures, a

DOI: 10.1021/acsnano.9b00395
ACS Nano 2019, 13, 5541−5548

testing set was built that consisted of a mechanical performance testing system for pressure control and a digital source meter for power supply along with electrical response recording. The a-PAN/G-based sensor (using p-PDMS with pattern #1) showed a steady response to each static pressure from 50 to 6000 Pa (Figure 4d), indicating that the resistances remained constant. From the pattern of the slope changes under different pressure, when the applied pressure changes within 1.8 kPa, there were a large amount of changes in the resistances, and that change became less obvious when the applied pressure was larger than 2 kPa.

The above observations could be more intuitive by measuring the change of the sensor output current ($\Delta I/I_0$) under a range of applied pressures. As shown in Figure 4e under various dynamic pressures, the a-PAN/G-film-based pressure sensor revealed stable and repeatable responses. In Figure 4f, the $\Delta I/I_0$ of three sensors with different substrate surface roughness are shown. It was shown that the sensor using p-PDMS substrates exhibited $\Delta I/I_0$ larger than that using flat PDMS (roughness ~2 μm). Sensitivity of the piezoresistive sensor is generally defined as $S = \mathrm{d}(\Delta I/I_0)/\mathrm{d}(P)$, where ΔI is the change in current and P is the applied pressure. As can be seen in Figure S13, all of the $\Delta I/I_0$–P plots were composed of more than one region. The sensitivity of the sensor with pattern #1 was about 74.8 kPa^{-1}, as the applied pressure was lower than 0.7 kPa, and 0.88 kPa^{-1} under higher applied pressure. For the sensor with pattern #2, the plot exhibited high linearity under 1200 Pa and the sensitivity was about 44.5 kPa^{-1} in the same region (<1200 Pa). For comparison, the sensitivities of the sensor with a flat surface were 20.47 kPa^{-1} (<500 Pa) and 0.18 kPa^{-1} (500–9000 Pa), indicating that the structure of the substrate directly affects the performance of the pressure sensor. To demonstrate the vital necessity of two-layered face-to-face a-PAN/G films, in addition to the a-PAN/G-film-based active material, annealed PAN nanofibers as an interlayer between graphene and PDMS (G/PAN/PDMS), annealed PAN nanofibers only, and graphene only were also used to fabricate pressure sensors as contrasts. It is shown in Figure S14 that the sensor with a-PAN/G/p-PDMS structure had sensitivity superior to that of other structures. We attributed the relatively high sensitivity to multistage contacts of two sensor electrodes. When a small amount of pressure was applied on the device, PAN fibers began to touch each other, leading to a strong increase in current. Then two a-PAN/G films near the peak structure of the substrate were touching each other. As pressure increases, further deformation with the elastic substrates occurs, giving rise to the progressive increase of the contact area of two a-PAN/G layers. Reliability and stability are also common aspects of concern for evaluating pressure sensors. The sensor showed a long-term reliable operation for up to 5500 cycles under a pressure of about 600 Pa (Figure 4g). Although monolayer graphene film usually tends to crack under applied stress,[3,26] the conductive PAN fiber constructed network provides additional conductive pathways when large deformation occurs and ensures the proper and continuous work of the sensor (Figure S15).

The pressure sensor based on a-PAN/G/p-PDMS #1 could respond to a subtle pressure of one and several water droplets (Figure S16a), whose pressure could be calculated to be about 2 and 4 Pa. Small vibration motions such as acoustic vibration signals could also be detected by this pressure sensor. Different sounds of letters "P", "K", and "U" were recorded by putting the pressure sensor on a speaker (Figure S16b). The signal spikes of the same letter appeared very similar, which might be further used in speech recognition after data processing. For transparent flexible pressure sensors, one of the most important applications should be attachment on curved surfaces that need constant observations. Monitoring of human physiological signals, such as pulse detection, is one of the examples that is of great importance for special populations, such as aged people, patients with chronic diseases, *etc*. The a-PAN/G-based transparent flexible pressure sensor attached to the wrist was used for autodetection of the pulse signal and allowed real-time observation of skin or blood vessel appearance (Figure S17a). Because the device may be attached to the skin for a relatively long period of time, the transparency feature of the device would help the timely observation of allergic reactions and wound healing processes. To detect pressure changes, a base pressure was needed, which could be introduced by simply using a hand to hold the sensor or using the polyurethane film dressing to affix the sensor on the radial artery of the wrist. Variations in pressure associated with pulse led to changes in current (I), which were recorded and presented in Figure 4h. Dressing helped fix the sensor tightly so that the I was higher and the signal was more stable than that of sensors being held gently by hand. From the single typical individual wave extracted (Figure S17b), the peaks were clearly distinguishable. These peak were labeled as P, T, and D, which are reported as the early systolic shoulder/peak, late systolic shoulder/peak, and dicrotic wave.[41,42] The results indicated that the a-PAN/G-film-based pressure sensor can be used to monitor subtle human biomedical signals and could be used as a key part of wearable diagnostic devices with further real-time wave analysis.

The best overall performance of the sensors, such as sensitivity, signal stability, power system compatibility, and operating voltage for measurements above, remains at 0.5 V. Actually, the sensor based on PAN/G could work normally under low voltage such as 0.01–0.05 V, as well. As shown in Figure S18a, current responses of the PAN/G/p-PDMS #1 pressure sensor under three different relatively low voltages are all workable. Figure S18b shows that under the periodic loading of pressure from 0 to 500 Pa, by using operating voltage of 0.01, 0.03, and 0.05 V, the signal peaks were quite stable and clear, proving the small signal stability which is critical to the real use of the device for calibration concerns. One potential problem is the appearance of double peaks in Figure S18b under 0.01 V, which may cause problems in automatic signal processing for practical applications. The origin of it was supposed to be the output voltage noise from the source meter. This could be confirmed by the program-controlled constant output voltage of 0.01, 0.03, and 0.05 V (Figure S19) that we measured.

CONCLUSION

In conclusion, we have designed and fabricated an annealed PAN nanofiber reinforced graphene film with enhanced conductivity and mechanical strength. Meanwhile, it maintained its high transparency (≥94%, 600 nm). This a-PAN/G film could be transferred in a large area without extra polymer assistance. Furthermore, its Young's modulus measured and calculated by nanoindentation is up to 1.04 ± 0.08 TPa. Combined with the patterned PDMS substrate, the a-PAN/G film was used as an active material for wearable pressure sensors. The additional conductive paths of nanofibers contribute to the conductivity stability under deformation

DOI: 10.1021/acsnano.9b00395
ACS Nano 2019, 13, 5541–5548

introduced by pressure. The sensors exhibited high sensitivity, low detection limit, low energy consumption, and excellent stability. Further, we applied these sensors to versatile applications, such as acoustic vibrations and pulse wave detection, in which the sensors showed excellent performances. Thus, the a-PAN/G film as a transparent conductive material could be very valuable for versatile applications of wearable electronics and smart gadgets in the near future.

EXPERIMENTAL SECTION

Fabrication of a-PAN/G Film. After the electrochemical polishing of Cu foil (98% purity, 25 μm thick, Alfa Aesar), the copper foil was placed in the furnace. Heating (50−200 sccm H_2) and annealing processes were conducted, followed by the programmed carbon source feeding for rapid growth of large domain sized graphene film. The graphene/copper foil sample was taken out of the furnace after being cooled and was put under the needle tip of the electrospinning machine. Polyacrylonitrile (10 wt %, MW = 1.5×10^5 g mol^{-1}, J&K Scientific) in DMF was electrospun onto the graphene film for 6 min with a 10 kV potential. The a-PAN/G/copper foil sample was put back into the furnace and annealed (heating speed of 5−15 °C/min) at 200−1000 °C for 0.5−1 h. The parameters used in the whole preparation process of the a-PAN/G films were sufficiently optimized. More specific descriptions are provided in the Supporting Information.

Characterizations. SEM characterizations were done using a Hitachi S-4800 with 5−30 kV acceleration voltage. Selected area electron diffraction measurements were performed using a FEI Tecnai F30 with an acceleration voltage of 300 kV. The optical microscopy images were obtained using an Olympus DX51 microscope. Raman spectra were measured using a Jobin Yvon LabRAM HR 800UV with a 25 mW, 514.5 nm laser. A semiconductor analyzer (Keithley, SCS-4200) was used to measure the electrical properties of PAN nanofibers. The sheet resistances of the a-PAN/G and PAN/G films were measured using a four-probe resistance measuring meter (Guangzhou 4-probe Tech Co. Ltd., RTS-4) based on a four-point probe method to eliminate contact resistance. X-ray photoelectron spectroscopy characterizations were performed using Kratos Axis Ultra-DLD spectrophotometer and monochromatic Al X-ray at low pressures of 5×10^{-9} to 1×10^{-8} Torr. The transmittance was measured by a UV−vis−NIR PerkinElmer Lambda 950 spectrophotometer. 3D profile mapping was acquired by 3D optical surface profiler ZYGO NexView. Surface profiles were measured by atomic force microscopy (Bruker Dimension icon, scansyst mode, scansyst air tip). Details of the nanoindentation process are described in the Supporting Information.

Testing of the Pressure Sensors. A Shimadzu AGS-X mechanical performance testing system was used to control and apply the programed pressure. Digital source meters (Keithley 2400) were used to control the applied voltage and record the current change during the pressure applied on the sensor.

ASSOCIATED CONTENT

Supporting Information

The Supporting Information is available free of charge on the ACS Publications website at DOI: 10.1021/acsnano.9b00395.

Materials and methods, supplementary text, and Figures S1−S20 (PDF)

AUTHOR INFORMATION

Corresponding Authors

*E-mail: hlpeng@pku.edu.cn.
*E-mail: weidi-cnc@pku.edu.cn.
*E-mail: zfliu@pku.edu.cn.

ORCID

Yingying Zhang: 0000-0002-8448-3059
Hailin Peng: 0000-0003-1569-0238
Zhongfan Liu: 0000-0003-0065-7988

Author Contributions

H.R. and L.Z. contributed equally to this work. Z.L., D.W., and H.P. designed the experimental part of the project. H.R. and L.Z. realized the fabrication of nanofiber-reinforced graphene films. H.R., L.C., J.S., and X.G. did the characterizations of as-fabricated a-PAN/G films and annealed PAN fibers. L.Z and G.W. performed the mechanical measurement. H.R. and Z.T. made the gear shaped electrode devices and carried out fiber conductivity measurements. H.R. designed the pressure sensor, and H.R. and K.L. fabricated the sensors. H.R. performed the characterizations and tests of the sensors, and M.J., L.Z., and Y.Z. helped analyze the results. H.R., L.Z., D.W., and Z.L. co-wrote the manuscript. All the authors participated in the data analysis.

Funding

This work was financially supported by the National Basic Research Program of China (Nos. 2016YFA0200103 and 2014CB932500) and the National Natural Science Foundation of China (Nos. 51432002 and 51520105003).

Notes

The authors declare no competing financial interest.

ACKNOWLEDGMENTS

We thank X. Liu and Z.Q. Wang for instrumental advice on this work.

REFERENCES

(1) Ahn, J.-H.; Hong, B. H. Graphene for Displays That Bend. *Nat. Nanotechnol.* **2014**, *9*, 737.
(2) Bae, S.; Kim, H.; Lee, Y.; Xu, X.; Park, J.-S.; Zheng, Y.; Balakrishnan, J.; Lei, T.; Ri Kim, H.; Song, Y. I.; et al. Roll-to-Roll Production of 30-Inch Graphene Films for Transparent Electrodes. *Nat. Nanotechnol.* **2010**, *5*, 574.
(3) Liu, N.; Chortos, A.; Lei, T.; Jin, L.; Kim, T. R.; Bae, W.-G.; Zhu, C.; Wang, S.; Pfattner, R.; Chen, X.; et al. Ultratransparent and Stretchable Graphene Electrodes. *Sci. Adv.* **2017**, *3*, No. e1700159.
(4) Cao, Q.; Hur, S. H.; Zhu, Z. T.; Sun, Y.; Wang, C. J.; Meitl, M. A.; Shim, M.; Rogers, J. A. Highly Bendable, Transparent Thin-Film Transistors That Use Carbon-Nanotube-Based Conductors and Semiconductors with Elastomeric Dielectrics. *Adv. Mater.* **2006**, *18*, 304−309.
(5) Artukovic, E.; Kaempgen, M.; Hecht, D.; Roth, S.; Grüner, G. Transparent and Flexible Carbon Nanotube Transistors. *Nano Lett.* **2005**, *5*, 757−760.
(6) Chen, T.; Peng, H.; Durstock, M.; Dai, L. High-Performance Transparent and Stretchable All-Solid Supercapacitors Based on Highly Aligned Carbon Nanotube Sheets. *Sci. Rep.* **2015**, *4*, 3612.
(7) Yang, Y.; Jeong, S.; Hu, L.; Wu, H.; Lee, S. W.; Cui, Y. Transparent Lithium-Ion Batteries. *Proc. Natl. Acad. Sci. U. S. A.* **2011**, *108*, 13013−13018.
(8) Gao, Y.; Zhou, Y.; Xiong, W.; Jiang, L.; Mahjouri-Samani, M.; Thirugnanam, P.; Huang, X.; Wang, M.; Jiang, L.; Lu, Y. Transparent, Flexible, and Solid-State Supercapacitors Based on Graphene Electrodes. *APL Mater.* **2013**, *1*, 012101.
(9) Kirsch, N. J.; Vacirca, N. A.; Plowman, E. E.; Kurzweg, T. P.; Fontecchio, A. K.; Dandekar, K. R. Optically Transparent Conductive Polymer RFID Meandering Dipole Antenna, RFID. *2009 IEEE International Conference*, 2009; pp 278−282.
(10) Yao, Y.; Yu, J.; Chen, X. Study on the Optically Transparent Near-Field and Far-Field RFID Reader Antenna. *Int. J. Antenn. Propag.* **2014**, *2014*, 1.

DOI: 10.1021/acsnano.9b00395
ACS Nano 2019, 13, 5541−5548

(11) Yang, B. D.; Oh, J. M.; Kang, H. J.; Park, S. H.; Hwang, C. S.; Ryu, M. K.; Pi, J. E. A Transparent Logic Circuit for RFID Tag in a-IGZO TFT Technology. *ETRI J.* **2013**, *35*, 610−616.
(12) Zhang, M.; Wang, C.; Wang, H.; Jian, M.; Hao, X.; Zhang, Y. Carbonized Cotton Fabric for High-performance Wearable Strain Sensors. *Adv. Funct. Mater.* **2017**, *27*, 1604795.
(13) Jian, M.; Xia, K.; Wang, Q.; Yin, Z.; Wang, H.; Wang, C.; Xie, H.; Zhang, M.; Zhang, Y. Flexible and Highly Sensitive Pressure Sensors Based on Bionic Hierarchical Structures. *Adv. Funct. Mater.* **2017**, *27*, 1606066.
(14) Shi, J.; Li, X.; Cheng, H.; Liu, Z.; Zhao, L.; Yang, T.; Dai, Z.; Cheng, Z.; Shi, E.; Yang, L.; et al. Graphene Reinforced Carbon Nanotube Networks for Wearable Strain Sensors. *Adv. Funct. Mater.* **2016**, *26*, 2078−2084.
(15) Kim, K. S.; Zhao, Y.; Jang, H.; Lee, S. Y.; Kim, J. M.; Kim, K. S.; Ahn, J.-H.; Kim, P.; Choi, J.-Y.; Hong, B. H. Large-Scale Pattern Growth of Graphene Films for Stretchable Transparent Electrodes. *Nature* **2009**, *457*, 706.
(16) Wang, X.; Gu, Y.; Xiong, Z.; Cui, Z.; Zhang, T. Silk-molded Flexible, Ultrasensitive, and Highly Stable Electronic Skin for Monitoring Human Physiological Signals. *Adv. Mater.* **2014**, *26*, 1336−1342.
(17) Hao, Y.; Bharathi, M.; Wang, L.; Liu, Y.; Chen, H.; Nie, S.; Wang, X.; Chou, H.; Tan, C.; Fallahazad, B.; et al. The Role of Surface Oxygen in the Growth of Large Single-Crystal Graphene on Copper. *Science* **2013**, *342*, 720−723.
(18) Boyd, D.; Lin, W.-H.; Hsu, C.-C.; Teague, M.; Chen, C.-C.; Lo, Y.-Y.; Chan, W.-Y.; Su, W.-B.; Cheng, T.-C.; Chang, C.-S.; et al. Single-Step Deposition of High-Mobility Graphene at Reduced Temperatures. *Nat. Commun.* **2015**, *6*, 6620.
(19) Li, X.; Cai, W.; An, J.; Kim, S.; Nah, J.; Yang, D.; Piner, R.; Velamakanni, A.; Jung, I.; Tutuc, E.; et al. Large-Area Synthesis of High-Quality and Uniform Graphene Films on Copper Foils. *Science* **2009**, *324*, 1312−1314.
(20) Lin, L.; Li, J.; Ren, H.; Koh, A. L.; Kang, N.; Peng, H.; Xu, H.; Liu, Z. Surface Engineering of Copper Foils for Growing Centimeter-Sized Single-Crystalline Graphene. *ACS Nano* **2016**, *10*, 2922−2929.
(21) Chen, Y.; Gong, X. L.; Gai, J. G. Progress and Challenges in Transfer of Large-Area Graphene Films. *Adv. Sci.* **2016**, *3*, 1500343.
(22) Chae, S. H.; Yu, W. J.; Bae, J. J.; Duong, D. L.; Perello, D.; Jeong, H. Y.; Ta, Q. H.; Ly, T. H.; Vu, Q. A.; Yun, M.; et al. Transferred Wrinkled Al_2O_3 for Highly Stretchable and Transparent Graphene-Carbon Nanotube Transistors. *Nat. Mater.* **2013**, *12*, 403.
(23) Jang, H.; Park, Y. J.; Chen, X.; Das, T.; Kim, M. S.; Ahn, J. H. Graphene-based Flexible and Stretchable Electronics. *Adv. Mater.* **2016**, *28*, 4184−4202.
(24) Lin, Y.-C.; Lu, C.-C.; Yeh, C.-H.; Jin, C.; Suenaga, K.; Chiu, P.-W. Graphene Annealing: How Clean Can It Be? *Nano Lett.* **2012**, *12*, 414−419.
(25) Ahn, Y.; Kim, H.; Kim, Y.-H.; Yi, Y.; Kim, S.-I. Procedure of Removing Polymer Residues and Its Influences on Electronic and Structural Characteristics of Graphene. *Appl. Phys. Lett.* **2013**, *102*, 091602.
(26) Hacopian, E. F.; Yang, Y.; Ni, B.; Li, Y.; Li, X.; Chen, Q.; Guo, H.; Tour, J. M.; Gao, H.; Lou, J. Toughening Graphene by Integrating Carbon Nanotubes. *ACS Nano* **2018**, *12*, 7901−7910.
(27) Lee, Y.; Bae, S.; Jang, H.; Jang, S.; Zhu, S.-E.; Sim, S. H.; Song, Y. I.; Hong, B. H.; Ahn, J.-H. Wafer-Scale Synthesis and Transfer of Graphene Films. *Nano Lett.* **2010**, *10*, 490−493.
(28) Zhang, Z.; Du, J.; Zhang, D.; Sun, H.; Yin, L.; Ma, L.; Chen, J.; Ma, D.; Cheng, H.-M.; Ren, W. Rosin-Enabled Ultraclean and Damage-Free Transfer of Graphene for Large-Area Flexible Organic Light-Emitting Diodes. *Nat. Commun.* **2017**, *8*, 14560.
(29) Yan, Z.; Peng, Z.; Casillas, G.; Lin, J.; Xiang, C.; Zhou, H.; Yang, Y.; Ruan, G.; Raji, A.-R. O.; Samuel, E. L.; et al. Rebar Graphene. *ACS Nano* **2014**, *8*, 5061−5068.
(30) Lin, L.; Sun, L.; Zhang, J.; Sun, J.; Koh, A. L.; Peng, H.; Liu, Z. Rapid Growth of Large Single-Crystalline Graphene *via* Second Passivation and Multistage Carbon Supply. *Adv. Mater.* **2016**, *28*, 4671−4677.
(31) Ren, H.; Wang, H.; Lin, L.; Tang, M.; Zhao, S.; Deng, B.; Priydarshi, M. K.; Zhang, J.; Peng, H.; Liu, Z. Rapid Growth of Angle-Confined Large-Domain Graphene Bicrystals. *Nano Res.* **2017**, *10*, 1189−1199.
(32) Xue, T. J.; McKinney, M. A.; Wilkie, C. A. The Thermal Degradation of Polyacrylonitrile. *Polym. Degrad. Stab.* **1997**, *58*, 193−202.
(33) Jain, M. K.; Abhiraman, A. Conversion of Acrylonitrile-Based Precursor Fibres to Carbon Fibres. *J. Mater. Sci.* **1987**, *22*, 278−300.
(34) Lee, C.; Wei, X.; Kysar, J. W.; Hone, J. Measurement of the Elastic Properties and Intrinsic Strength of Monolayer Graphene. *Science* **2008**, *321*, 385−388.
(35) López-Polín, G.; Gómez-Navarro, C.; Parente, V.; Guinea, F.; Katsnelson, M. I.; Perez-Murano, F.; Gómez-Herrero, J. Increasing the Elastic Modulus of Graphene by Controlled Defect Creation. *Nat. Phys.* **2015**, *11*, 26−31.
(36) Lin, Q.-Y.; Zeng, Y.-H.; Liu, D.; Jing, G. Y.; Liao, Z.-M.; Yu, D. Step-by-step Fracture of Two-Layer Stacked Graphene Membranes. *ACS Nano* **2014**, *8*, 10246−10251.
(37) Lee, G.-H.; Cooper, R. C.; An, S. J.; Lee, S.; Van Der Zande, A.; Petrone, N.; Hammerberg, A. G.; Lee, C.; Crawford, B.; Oliver, W.; et al. High-Strength Chemical-Vapor-Deposited Graphene and Grain Boundaries. *Science* **2013**, *340*, 1073−1076.
(38) Dahiya, R. S.; Metta, G.; Valle, M.; Sandini, G. Tactile Sensing—from Humans to Humanoids. *IEEE Trans. Robotics.* **2010**, *26*, 1−20.
(39) Lin, L.; Xie, Y.; Wang, S.; Wu, W.; Niu, S.; Wen, X.; Wang, Z. L. IEEE Trans. RoboticsTriboelectric Active Sensor Array for Self-Powered Static and Dynamic Pressure Detection and Tactile Imaging. *ACS Nano* **2013**, *7*, 8266−8274.
(40) Park, J.; Lee, Y.; Hong, J.; Lee, Y.; Ha, M.; Jung, Y.; Lim, H.; Kim, S. Y.; Ko, H. IEEE Trans. RoboticsTactile-Direction-Sensitive and Stretchable Electronic Skins Based on Human-Skin-Inspired Interlocked Microstructures. *ACS Nano* **2014**, *8*, 12020−12029.
(41) Takazawa, K.; Kobayashi, H.; Shindo, N.; Tanaka, N.; Yamashina, A. IEEE Trans. RoboticsRelationship Between Radial and Central Arterial Pulse Wave and Evaluation of Central Aortic Pressure Using the Radial Arterial Pulse Wave. *Hypertens. Res.* **2007**, *30*, 219−228.
(42) Chen, C.-H.; Ting, C.-T.; Nussbacher, A.; Nevo, E.; Kass, D. A.; Pak, P.; Wang, S.-P.; Chang, M.-S.; Yin, F. C. Validation of Carotid Artery Tonometry as a Means of Estimating Augmentation Index of Ascending Aortic Pressure. *Hypertension* **1996**, *27*, 168−175.

DOI: 10.1021/acsnano.9b00395
ACS Nano 2019, 13, 5541−5548